Progress in Biophysics and Molecular Biology 115 (2014) 314–327

Contents lists available at ScienceDirect

Progress in Biophysics and Molecular Biology

journal homepage: www.elsevier.com/locate/pbiomolbio

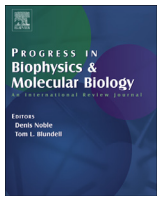

Original research

Living cardiac tissue slices: An organotypic pseudo two-dimensional model for cardiac biophysics research

Ken Wang [a], Derek Terrar [b], David J. Gavaghan [a], Razik Mu-u-min [c], Peter Kohl [a, d], Christian Bollensdorff [c, d, *]

[a] Computer Science Department, University of Oxford, Wolfson Building, Parks Road, Oxford, OX1 3QD, UK
[b] Department of Pharmacology, University of Oxford, Mansfield Road, Oxford OX1 3QT, UK
[c] Qatar Cardiovascular Research Center, Qatar Foundation Qatar Foundation, PO Box 5825, Doha, Qatar
[d] Harefield Heart Science Centre, National Heart and Lung Institute, Imperial College London, Harefield, Middlesex, UB9 6JH, UK

ARTICLE INFO

Article history:
Available online 11 August 2014

Keywords:
Mechano-electric feedback
Optical mapping
Axial stretch
Multi-parametric

ABSTRACT

Living cardiac tissue slices, a pseudo two-dimensional (2D) preparation, have received less attention than isolated single cells, cell cultures, or Langendorff-perfused hearts in cardiac biophysics research. This is, in part, due to difficulties associated with sectioning cardiac tissue to obtain live slices. With moderate complexity, native cell-types, and well-preserved cell–cell electrical and mechanical interconnections, cardiac tissue slices have several advantages for studying cardiac electrophysiology. The trans-membrane potential (V_m) has, thus far, mainly been explored using multi-electrode arrays. Here, we combine tissue slices with optical mapping to monitor V_m and intracellular Ca^{2+} concentration ($[Ca^{2+}]_i$). This combination opens up the possibility of studying the effects of experimental interventions upon action potential (AP) and calcium transient (CaT) dynamics in 2D, and with relatively high spatio-temporal resolution.

As an intervention, we conducted proof-of-principle application of stretch. Mechanical stimulation of cardiac preparations is well-established for membrane patches, single cells and whole heart preparations. For cardiac tissue slices, it is possible to apply stretch perpendicular or parallel to the dominant orientation of cells, while keeping the preparation in a constant focal plane for fluorescent imaging of in-slice functional dynamics. Slice-to-slice comparison furthermore allows one to assess transmural differences in ventricular tissue responses to mechanical challenges. We developed and tested application of axial stretch to cardiac tissue slices, using a manually-controlled stretching device, and recorded V_m and $[Ca^{2+}]_i$ by optical mapping before, during, and after application of stretch.

Living cardiac tissue slices, exposed to axial stretch, show an initial shortening in both AP and CaT duration upon stretch application, followed in most cases by a gradual prolongation of AP and CaT duration during stretch maintained for up to 50 min. After release of sustained stretch, AP duration (APD) and CaT duration reverted to shorter values.

Living cardiac tissue slices are a promising experimental model for the study of cardiac mechano-electric interactions. The methodology described here can be refined to achieve more accurate control over stretch amplitude and timing (e.g. using a computer-controlled motorised stage, or by synchronising electrical and mechanical events) and through monitoring of regional tissue deformation (e.g. by adding motion tracking).

Abbreviations: AP, Action potential; APD, Action potential duration; APDxx, Action potential duration at xx % repolarisation; ATP, Adenosine triphosphate; CaT, Intracellular Ca^{2+} transient; CaTyy, Calcium transient duration at yy % decay; $[Ca^{2+}]_i$, Intracellular free Ca^{2+} concentration; LV, Left ventricle/ventricular; MEF, Mechano-electric feedback; $[Na^+]_i$, Intracellular free Na^+ concentration; RV, Right ventricle/ventricular; SAC, Stretch activated channels; SD, Standard deviation; V_m, Trans-membrane potential.

* Corresponding author. Qatar Cardiovascular Research Center, Qatar Foundation, PO Box 5825, Doha, Qatar. Tel.: +974 4454 5814.
E-mail addresses: ken.wang@dtc.ox.ac.uk (K. Wang), derek.terrar@pharm.ox.ac.uk (D. Terrar), david.gavaghan@cx.ox.ac.uk (D.J. Gavaghan), rmuumin@qf.org.qa (R. Mu-u-min), p.kohl@imperial.ac.uk (P. Kohl), cbollensdorff@qf.org.qa, christian@bollensdorff.de (C. Bollensdorff).

http://dx.doi.org/10.1016/j.pbiomolbio.2014.08.006

1. Introduction

Living cardiac tissue slices as an *ex vivo* model system for the study of cardiac biophysics and biology have been gaining popularity in recent years. Recent examples include the study of cardiac electrophysiology, mechanics, and pharmacology (Bussek et al., 2009; Camelliti et al., 2011; Brandenburger et al., 2012). Cardiac tissue slices have unique advantages over other cardiac preparations, as they combine partial preservation of tissue morphology with improved control and observation of structure-function relations (de Boer et al., 2009). Their pseudo-two-dimensional (2D) nature makes them a promising candidate also for studying cardiac mechano-electrics using optical techniques. Here, we illustrate in a proof-of-principle study that optical mapping of trans-membrane potential (V_m) and intracellular 'free' Ca^{2+} concentration ($[Ca^{2+}]_i$) can be conducted in live ventricular tissue slices, and be combined with mechanical stimulation to assess mechano-electric feedback (MEF) effects through comparing action potentials (AP) and Ca^{2+} transients (CaT) before, during, and after application of stretch.

1.1. Investigation of mechano-electric feedback: preparations and methodologies

MEF is the process whereby a change in the mechanical environment influences the electrical signal in excitable tissues or cells (Lab, 1996, 1999; Kohl et al., 1999; Kohl et al., 2006); as recently reviewed in a focussed issue of PBMB (Kohl et al., 2012). Disturbances in the normal mechanical activity of the heart, whether acute (e.g. due to a precordial impact (Kohl et al., 2001; Maron et al., 2002)) or sustained (e.g. in ventricular volume overload (Eckardt et al., 2001; Quinn, 2014)), can result in stretch-induced arrhythmias. Interestingly, mechanically induced cardioversion has also been reported upon acute pre-cordial stimulation (Madias et al., 2009; Pellis et al., 2009), or by (temporary) removal of sustained stretch of the chronically overloaded heart (Waxman et al., 1980), highlighting the clinical relevance of cardiac MEF research. Further studies into the effects of stretch on the electrophysiological properties of cardiac tissue are needed to unlock additional insight into the mechanisms of cardiac mechano-electric cross-talk.

Ex vivo research into cardiac MEF has been carried out on different experimental models. The most commonly used preparations are single isolated cardiomyocytes (e.g. (Le Guennec et al., 1991)), cell cultures (e.g. (Zhang et al., 2008)), trabecular and papillary muscle preparations (e.g. (Nakagawa et al., 1988)), and Langendorff perfused whole hearts (e.g. (Pathak, 1957)). Scaling up from single cell to whole heart, preparations reflect the *in situ* setting more closely, albeit at the cost of (i) a reduction in the ability to 'pin-point' underlying structural substrates and mechanisms, and (ii) reduced experimental control over the biophysical environment.

A number of methods for mechanical stimulation have been developed, in a preparation-dependent manner. For single isolated cells, stretch can be achieved by attaching carbon fibres (Le Guennec et al., 1990; Le Guennec et al., 1991) to both ends of a cell and stretching the cell by increasing the distance between the fibres (Belus and White, 2003; Iribe et al., 2009), potentially even mimicking intra-cardiac force-length loop behaviour (Iribe et al., 2007; Bollensdorff et al., 2011). Single cardiomyocytes can also be mechanically manipulated by a pair of glass pipettes (Tung and Zou, 1995; Zeng et al., 2000), a glass pipette and a glass stylus (Kamkin et al., 2000), or be glued to a pair of glass rods (Prosser et al., 2011). For cell cultures, cells can be seeded and cultured on deformable elastomers, where mechanical manipulation is achieved by deforming (stretching) the membrane (Gopalan et al., 2003; Camelliti et al., 2006; Zhang et al., 2008). Isolated trabecular and papillary muscle can be suspended between actuator/force transducer pairs for stress-strain control in single (Allen and Kurihara, 1982; Allen and Kentish, 1988; ter Keurs et al., 2008) and paired muscle preparations (Markhasin et al., 2003; see also Solovyova et al. 2014). In Langendorff perfused whole heart, fluid-filled balloons, inserted into the ventricle, have been used to control ventricular loading conditions (Zabel et al., 1996). More classically, stretch can be applied to the isolated whole heart by attaching weights or a force transducer to the apex (Langendorff, 1895; Botchway et al., 2003). Alternatively, localized tissue impact equipment has been developed to study mechanisms of mechanically-induced sudden cardiac arrest in the isolated whole heart (Cooper et al., 2006).

1.2. MEF-related changes in action potential shape and duration in different preparations

Extensive studies have been carried out on all *ex vivo* preparations mentioned above, from single cell to whole heart, to investigate the effects of mechanical stimulation on AP shape and duration (APD). A selection of key results, grouped by preparation, is summarised below.

1.2.1. Isolated cardiomyocytes

Cardiomyocytes, isolated from ventricular or atrial tissue of different species, have been used to study MEF. V_m was monitored via patch clamp (White et al., 1993; Tung and Zou, 1995; Kamkin et al., 2000; Zeng et al., 2000; Zhang et al., 2000; Belus and White, 2003; Riemer and Tung, 2003; Kohl et al., 2006) or optical mapping (Nishimura et al., 2006).

In guinea pig ventricular myocytes (stretch applied by carbon fibres), both prolongation (by 9%) (Belus and White, 2003) or shortening (by 4%) (White et al., 1993) of APD were reported after stretch. The difference between these observations may be caused by different temperatures used in the experiments (Belus and White, 2003), or by diverse effects on sub-cellular mechano-sensors (e.g. stretch-activated ion channels [SAC] or Ca^{2+} handling) which can be affected differentially by various recording techniques (ruptured patch *vs*. permeabilised patch *vs*. sharp electrodes (Kohl et al., 1998)). In another study where stretch was applied with a patch pipette and a glass stylus (Kamkin et al., 2000), cross-over of AP repolarisation was observed after stretch, with a decrease in APD at 20% repolarisation (APD20) and an increase in APD at 90% repolarisation (APD90). This highlights that the level of AP repolarisation, at which stretch effects are analysed, can affect observed outcomes.

Stretch parameters may affect findings as well. Thus, an increase in APD at 50% repolarisation (APD50) and APD90 was observed in rat cardiomyocytes (both ventricular and atrial) when stretching cells with a pair of glass pipettes (Zeng et al., 2000; Zhang et al., 2000). In a subsequent study on rat ventricular myocytes, timing and speed of stretch were tightly controlled, and it was observed that timing relative to the AP cycle, amplitude of stretch, and the speed at which stretch is applied all influence results. Here, stretch applied only during the early phase of an AP did not change APD, while stretch at later stages prolonged APD. Also, a positive correlation between the level of depolarisation and the speed of stretch application was identified (Nishimura et al., 2006).

Partially contrasting results were reported for frog ventricular myocytes. Shortening (Tung and Zou, 1995), prolongation (in 3 out of 252 stretch trials), and no significant change in APD (249 out of 252 stretch trials) were observed after application of uniaxial stretch (Riemer and Tung, 2003).

Stretch application to isolated sino-atrial node pacemaker cells identified a reduction in the absolute values of maximum systolic and maximum diastolic potentials, combined with an increase in spontaneous diastolic depolarization and early systolic

repolarization rates (Cooper et al., 2000). This could explain species differences in SAN pacemaker responses to stretch, as the relative durations of spontaneous diastolic depolarization and early repolarization vary as a function of background AP shape (Cooper and Kohl, 2005).

1.2.2. Cell culture

Compared to other preparations, a relatively small number of investigations involved acute stretch of cell cultures during electrophysiological research. Cultures from cardiac tissue explants are usually based on neonatal rat ventricular myocytes. In this model system, an increase in APD after stretch was described (Zhang et al., 2008). Another study used HL-1 (cardiomyocyte-like) cells, and also found a slight prolongation in APD with stretch (Tsai et al., 2011). Using a fluid-jet based approach and observing responses by voltage-sensitive dye application, the lab of Les Tung showed that mechanical stimulation can give rise to focal excitation and re-entry (Kong et al., 2005). More recently, the same team explored MEF in cell cultures by relying on the cell's intrinsic activity as a mechanical stimulus, concluding that the interaction of myocytes and non-myocytes may provide additional pathways for mechanical modulation of cardiac conduction, in particular in injured tissue (Thompson et al., 2011).

1.2.3. Trabecular and papillary muscles

A number of studies investigated MEF in trabecular and papillary muscle preparations. In these studies, sharp electrodes are commonly used to monitor V_m (Kaufmann et al., 1971b; Lab, 1980). Both shortening and prolongation of the AP were observed in cat papillary muscle, where it was shown that the effect of stretch upon the AP may depend on the mode of contraction, with increased APD during isotonic shortening, and APD reduction in isometric tension development (Kaufmann et al., 1971b). A clear shortening of APD was seen in frog ventricular tissue strips after application of stretch (Lab, 1980). During sustained stretch, dynamic changes in APD are observed in muscle preparations, with an initial drop in APD shortly after stretch application, followed by a gradual prolongation during sustained distension, associated with the so-called 'slow force response' (see section 1.3.2 and (Allen, 1975, 1977)). Interestingly, the 'duplex' model of two mechanically interacting cardiac tissue preparations shows that *in situ* even more complex patterns of APD (and contractility) changes have to be expected, depending on the highly dynamic interactions between ventricular regions that are exposed to heterogeneous stress-strain dynamics (Markhasin et al., 2012) and (Solovyova et al. 2014).

1.2.4. Isolated whole heart

In isolated rabbit heart, an increase in APD at 80% repolarisation (APD80) was observed by optical mapping when stretching the left ventricle (LV) with a liquid-filled balloon (Sung et al., 2003). Increased APD90 was also reported in canine hearts, when stretching the LV with a similar method (Franz et al., 1989). Interestingly, the former (rabbit heart) study reported no change in APD20, while the latter (canine) report demonstrated a reduction in APD20. In contrast, stretch-induced reductions in both APD50 and APD90 were seen in canine (Lerman et al., 1985, 2001) and frog hearts (Lab, 1978).

When applying stretch to the heart via increasing intraventricular balloon volume in a time-controlled manner, it was found that stretch during the plateau phase of the AP leads to transient repolarisation, while stretch applied late in systole or early in diastole can result in membrane depolarisation (Zabel et al., 1996). One study on embryonic fish heart showed that directionality of stretch application may also matter: AP prolongation was observed with stretch applied in parallel to the main atrio-ventricular axis, while transverse stretch had no effect on APD (Werdich et al., 2012). This suggests that, in addition to temporal parameters, spatial properties of mechanical stimulation may contribute to inconsistencies in the published results.

MEF has also been studied in rabbit hearts whose right ventricle (RV) was cut open to form a tissue flap composed of RV free wall (one side remained attached to the LV, the other was attached to an actuator). In this study, stretch induced excitation which could lead to ventricular re-entrant arrhythmias (Seo et al., 2010).

Thus, reported stretch-effects on the AP vary, with possible explanations linked to differences in background AP shape (species and myocardial cell type differences), stretch properties (amplitude and rate of change, directionality relative to cardiac tissue), experimental conditions (temperature, electrophysiological recording techniques), repolarisation level at which APD changes are reported (APD50 *vs*. APD80), and timing of observations (acute or steady-state), to name but a few.

1.3. Postulated mechanisms

In keeping with the varied results on stretch-induced changes in AP shape and duration, underlying mechanisms are also a subject of debate. We briefly review in the following subsections the two most frequently implicated contributors, whose activity can best be explored using approaches that combine V_m and $[Ca^{2+}]_i$ recordings.

1.3.1. Mechanisms involving stretch activated ion channels

Stretch activated channels (SAC) are a group of ion channels whose gating is regulated mainly by the mechanical environment. They were first discovered in chick skeletal muscle (Guharay and Sachs, 1984), and subsequently confirmed in mammalian heart (Craelius et al., 1988). Cardiac SAC are believed to play important roles in changing electrophysiological properties of myocytes in response to mechanical stretch (Bustamante et al., 1991; Hu and Sachs, 1997; Kohl and Sachs, 2001). Single channel and whole cell studies suggest that the SAC populations involved in cardiac MEF responses *in healthy tissue* preferentially conduct cations, although in a non-selective manner, and have voltage-independent activation (Sasaki et al., 1992; Zhang et al., 2000), with reversal potentials between 0 and -15 mV (Zeng et al., 2000). Other groups of cardiac mechano-sensitive ion channels include potassium-selective SAC (Kim, 1992) with reversal potentials negative to myocyte resting potentials, and cell-volume activated channels (Baumgarten and Clemo, 2003) such as chloride-selective channels with a reversal potential close to zero. Both potassium-SAC (Van Wagoner and Lamorgese, 1994) and cell volume-activated channels (Baumgarten and Clemo, 2003) are likely to become more important in pathological conditions, including myocardial ischaemia (for more detailed reviews, please see (Baumgarten, 2000) and (Reed et al., 2014)).

Activation of cation non-selective SAC at negative V_m (e.g. during diastole) induces an inward current that can depolarise the cell membrane (if SAC-activation is large enough). At positive V_m (e.g. during the AP plateau), an outward current is generated, which can speed-up the initial repolarisation phase (Zabel et al., 1996; Isenberg et al., 2005). Activation of these SAC during the early or the late phase of the AP can therefore lead to differential effects. This may explain early AP shortening, cross-over of AP repolarisation, and prolongation of the late AP, as well as the effects on pacemaker cell V_m described above.

These considerations are largely based on conceptual or computational projection (Kohl et al., 1998; Trayanova et al., 2004; Healy and McCulloch, 2005; Xie et al., 2009; Zhan and Xia, 2013) from SAC single channel properties, studied in expression systems, immature, or atrial cardiomyocytes, as well as in cardiac non-myocytes (Kamkin et al.,

2010) which may be electrically coupled to heart muscle cells (Camelliti et al., 2004; Kohl and Gourdie, 2014). 'The' cardiac SAC has remained elusive in studies of freshly isolated ventricular myocytes. It has been suggested, therefore, that SAC in mature cardiomyocytes of the ventricles may be hidden in membrane areas that are difficult to reach by patch-clamp approaches, such as the t-tubular system, caveolae, or the intercalated discs (Sachs, 2011).

That said, the theoretical projections are fully in keeping with data from research using pharmacological block of SAC, confirming their direct involvement in acute cardiac MEF effects. Blockers used include Gd^{3+} (Yang and Sachs, 1989), streptomycin (Belus and White, 2003), and GsMTx4 (Suchyna et al., 2000). Both Gd^{3+} and streptomycin are non-specific and can also block L type Ca^{2+} currents, Na^+/Ca^{2+} exchanger, or delayed rectifier K^+ currents (Ward et al., 2008). As a further note of caution, the efficacy as SAC-blockers in isolated cells and cultures, both of Gd^{3+} (Caldwell et al., 1998) and of streptomycin (Cooper and Kohl, 2005), may not be maintained in native tissue preparations, either because of precipitation in physiological buffer systems (Gd^{3+}), or because of apparent access restrictions to the site of action on/near SAC (streptomycin).

1.3.2. Mechanisms mediated by calcium handling pathways

Another mechanism for stretch-induced changes in cardiac electrophysiological properties is mechanical modulation of intracellular Ca^{2+} handling. Intracellular Ca^{2+} affects ion channel behaviour underlying currents such as the L-type Ca^{2+} current, the delayed rectifier K^+ current, or the Na^{2+}/Ca^{2+} exchanger, which in turn affect excitability, AP profile, and conduction (Lee et al., 1985; Lerman et al., 1985; Tohse, 1990; duBell et al., 1991; Janvier and Boyett, 1996). Stretch is known to alter Ca^{2+} handling in myocytes (Calaghan et al., 2003) and non-myocytes of the heart (Kiseleva et al., 1996), and this is regarded as another key contributor to cardiac MEF (McCulloch et al., 2013).

Studies in guinea pig ventricular myocytes, stretched by carbon fibres, have shown an increase in resting $[Ca^{2+}]_i$ (Le Guennec et al., 1991; White et al., 1993; Gannier et al., 1996). Similar research in rat atrial and ventricular myocytes found no influence of stretch on $[Ca^{2+}]_i$ (Hongo et al., 1996; Tavi et al., 1998; Alvarez et al., 1999). These opposite findings may be due to species differences, or inconsistencies in Ca^{2+} sensitive fluorescent dyes that were used to monitor $[Ca^{2+}]_i$. This later can be the case because altered cytosolic Ca^{2+} buffering affects $[Ca^{2+}]_i$. Buffer capacity is affected not only by the uptake/release balance of the sarcoplasmic reticulum, Ca^{2+} pump and Na^{2+}/Ca^{2+} exchanger (Youm et al., 2005), and Ca^{2+}-binding to contractile filaments (Moss and Fitzsimons, 2002), but also by the addition of fluorescent reporter dyes with their different Ca^{2+} affinities (Konishi and Berlin, 1993).

In terms of systolic behaviour, the 'classic' Frank-Starling effect of an immediate stretch-induced increase in contractility is generally assumed to *not* involve any significant change in CaT (Shiels and White, 2008). However, maintained stretch gives rise to an increase in CaT, and this is regarded as the mechanism underlying the slow force response – a further increase in contractility over time beyond the immediate Frank-Starling response (Allen and Kurihara, 1982).

A delicate interplay between Ca^{2+} mediated mechanism and sarcolemmal SAC has been reported. Both L-type Ca^{2+} channels (Belus and White, 2003) and intracellular Na^+ are involved in this (Youm et al., 2005). A decrease in L-type Ca^{2+} current was observed upon addition of the Ca^{2+}-chelator BAPTA (1,2-bis(o-aminophenoxy)ethane-N,N,N′,N′-tetraacetic acid) and of streptomycin, suggesting links between L-type Ca^{2+} current and SAC activation (Belus and White, 2003). Furthermore, increased intracellular free Na^+ concentration ($[Na^+]_i$) was seen upon mechanical stimulation of cardiomyocytes, and this has been attributed to SAC (Alvarez et al., 1999; Isenberg et al., 2003). This increase in $[Na^+]_i$ may help to raise $[Ca^{2+}]_i$ via indirect effects on the transport balance of the Na^+/Ca^{2+} exchanger (Gannier et al., 1994; Youm et al., 2005).

Finally, it is important to realise that SAC are not necessarily restricted to the sarcolemma. Both the sarcoplasmic reticulum (Iribe and Kohl, 2008; Iribe et al., 2009) and mitochondria (Belmonte and Morad, 2008a, 2008b) of cardiomyocytes appear to contain ion transport pathways that respond acutely to external mechanical stimuli. Other intracellular membrane compartments, such as the nuclear envelope, may be 'mechano-sensitive', too.

Thus, stretch affects cardiac Ca^{2+} handling, not only via sarcolemmal SAC-mediated ion flux alterations that can (directly or indirectly) alter $[Ca^{2+}]_i$, but also via direct mechanical effects on internal fluxes and buffer capacities. An added complication is the fact that observation of $[Ca^{2+}]_i$ requires addition of fluorescent dyes, which themselves are Ca^{2+}-buffers that alter the dynamics of the observed parameter.

1.4. Aim of this study

The range of varying results for stretch-induced changes in APD makes it difficult to establish the exact mechanisms underlying cardiac electrophysiological responses to mechanical stimulation. Variations in published results can be, in part at least, attributed to different techniques and experimental conditions used, as well as to type of stretch stimulus and species differences. Beyond these considerations, there is a chasm between the desire to study MEF in experimental models that are 'as physiological as possible', and the need to link functional observations to structural information in experimental models that are 'as simple as one can get away with' (Garny et al., 2005). In this study we explore, therefore, the suitability of live cardiac tissue slices as models for studying MEF, and establish a method to investigate the effects of axial stretch on V_m and CaT using multi-parametric optical mapping.

2. Material and methods

2.1. Heart preparation

New Zealand White rabbits (male, 1–2 kg) were humanely killed using an overdose of anaesthetics (70 mg/kg pentobarbital) in accordance with schedule 1 of the UK Home Office Animals (Scientific Procedures) Act of 1986. Hearts were quickly excised and perfused in Langendorff mode, at a rate of 15–20 mL/min, with bicarbonate-buffered solution (containing, [in mmol/L]: NaCl 123, $CaCl_2$ 1.8, KCl 5.4, $MgCl_2$ 1.2, NaH_2PO_4 1.4, $NaHCO_3$ 24, Glucose 10; bubbled with carbogen [95% O_2/5% CO_2]; pH 7.4 at 35 ± 2 °C). Prior to commencement of interventions, hearts were allowed to accommodate and reach a regular beating rate, usually of about 240 beats per minute.

2.2. Dye loading

The fluorescent dyes, di-4-ANBDQPQ (stock solution: 29 mmol/L in ethanol; University of Connecticut Health Center, USA) and Rhod-2 AM (stock solution: 1 mg/mL in DMSO; AAT Bioquest Inc., Sunnyvale, USA) were used to image V_m and CaT, respectively. The heart was loaded with the dyes by adding 20 μL of di-4-ANBDQPQ and 200 μL Rhod-2-AM stocks to the perfusion solutions, close to the aortic cannula. Dyes were applied in small volume steps over a period of 5 min. To ensure proper loading of the Ca^{2+} dye, the perfusate was re-circulated over a period of 40–60 min. In addition, 0.5 mmol/L probenicid, an anion exchanger blocker (Di Virgilio et al., 1990), was used. No reperfusion was necessary for the V_m

dye, but 2 μL of Pluronic F-127 (20% stock solution in DMSO; Life Technologies, Paisley, UK) was added for enhancement of dye uptake. The whole heart was imaged just prior to cutting of live tissue slices, to confirm proper dye loading and signal quality.

2.3. Slice preparation

Before tissue slicing, while continuing Langendorff perfusion, the bicarbonate buffered solution was replaced by HEPES buffered solution (containing [in mmol/L]: NaCl 140, $CaCl_2$ 1.8, KCl 5.4, $MgCl_2$ 1, Glucose 11, HEPES 5, BDM 10, probenecid 0.5, bubbled with medical grade 99.9% oxygen). For complete electromechanical uncoupling, 10 μmol/L blebbistatin was added in addition to BDM, and the heart was gently cooled down to room temperature. The LV and RV free walls were dissected and trimmed to fit the slicing stage of a high precision vibratome (7000smz tissue slicer; Campden Instruments Ltd., Loughborough, UK). Tissue blocks were glued onto the slicing stage, with the endocardium facing down, using a histoacryl tissue adhesive (Braun, Melsungen, Germany). Slices were cut at 350 μm thickness, near-parallel to the epicardial plane. During sectioning, the tissue was kept in ice-cold oxygenated HEPES buffered solution (pH = 7.4 at 4 °C). All slices were collected on PDMS blocks (polydimethylsiloxane Sylgard 184; Dowcorning, Midland, USA), and secured by tailor-made fine mesh covers, to keep track of the original slice orientation. Tissue sections were then returned to room temperature in blebbistatin-containing bicarbonate buffered solution (pH 7.4 at room temperature) allowing them to adapt for ~10 min. Finally, slices were gently warmed back up to body temperature (35 ± 2 °C) in blebbistatin-containing bicarbonate buffered solution, and incubated in these conditions for at least one hour to allow full recovery and stabilisation (for a more detailed description of the protocol and important technical hints see (Wang et al., 2014).

A reference V_m signal was taken from each slice before mounting onto the stretching device (Fig. 1A). For mounting, slices were placed on two (single-use) plastic sheets which were fixed onto the surface of a micromanipulator (one attached to the static, the other to the movable part). After placing the tissue slice in the desired direction, opposite edges of the slice were placed on a line of tissue glue (Braun, WPI, Hitchin, UK) on top of the plastic sheet. The assembly was then re-submerged into blebbistatin-containing bicarbonate buffered solution. During mounting, care was taken to keep slices at their 'slack' length, maintaining them moist at all times to avoid additional tissue damage. A scale-bar, mounted beside the slice, was used for quantification of stretch.

2.4. Optical mapping

Fig. 1B shows a schematic of the mapping set-up. For optical recordings, an EMCCD camera with 128 × 128 pixels (Evolve 128 Photometrics, Tucson, USA) was mounted above the stretching device on a height-adjustable holder. For illumination, we used two different sources: a red LED (LED-CBT-90-R; Chroma Technology, Bellows Falls, USA) with band-pass filter D640/20× (Chroma Technology) to excite the V_m dye, and a white LED (LED-CBT-90-W; Luminus Devices) with band-pass filter S555/25× (Chroma Technology) for the Ca^{2+} sensitive dye. For collection of fluorescent emission, a combination of two filters was used (ET585/50-800/200; Chroma Technology; and a 561 nm long-pass filter, BLP01-561R-25; Semrock, Rochester, USA) to ensure non-overlapping spectral bands for exclusion of excitation light and collection of emitted fluorescent signals. The V_m and Ca^{2+} measurements were taken in consecutive frame sequences at maximal resolution (128 × 128 pixels) and frame rate (525 Hz). Data were acquired with PVCAM Version 1.0.7 (courtesy of Prof Stefan Luther and Johannes Schröder-Scheteling, University of Göttingen, Germany).

The chamber accommodating the stretching device was kept in a larger heated bath to ensure temperature stability. The solution in the tissue chamber was bubbled with carbogen between measurements, to sustain oxygen content and pH.

2.5. Pacing approach

Tissue slices were stimulated with 2 platinum field-stimulation electrodes, placed on opposite sides of the tissue (direction of electrodes parallel to the direction of stretch).

Pacing was applied using a Myopacer (Ionoptix, Dublin, Ireland) with bipolar pulses of 2 ms duration, at voltages 1.5 times above threshold, usually between 5 and 20 V. The pacing frequency was set to 2 Hz. Stimulation was started before measurements to allow slices to adjust to the pacing rate. Usually two consecutive measurements were taken, and where possible both measurements

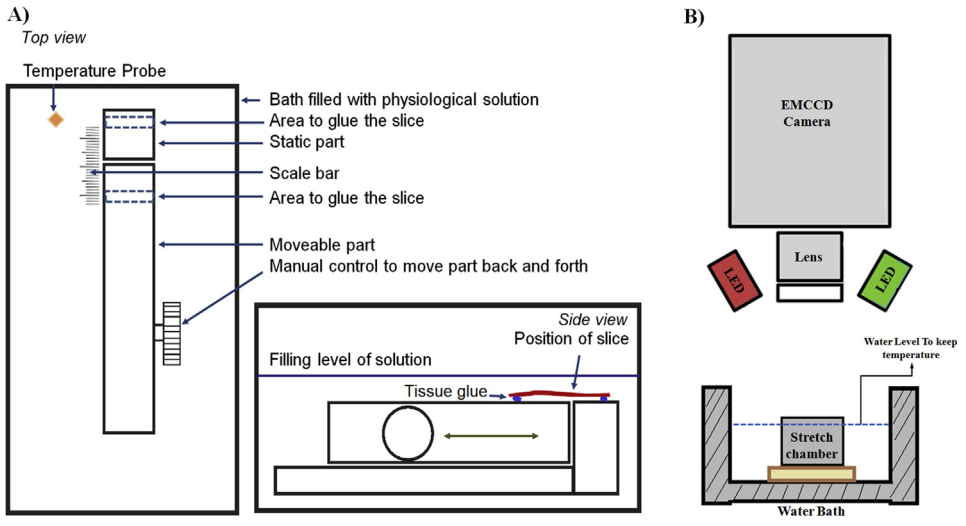

Fig. 1. Schematic illustration of the stretch chamber design with manual micromanipulator (A) and the optical mapping setup (B). The contact area between stretcher and slice was covered by plastic tape to avoid direct contact between tissue and metallic parts of the manipulator.

Table 1
Overview of cardiac tissue slices included in the analysis.

Slice	Rabbit	Preparation	Slice location	Time between stretch and first measurement	% Stretch	Stretch direction *vs.* main fibre direction
1	i	A	RV	<1 min	4.5	Not identified
2	ii	B	LV sub-epicardial	3 min	8.5	Perpendicular
3	ii	C	LV mid-myocardial	<1 min	6.9	Parallel
4	iii	D	LV sub-epicardial	~0.5 min	9.8	Perpendicular
4	iii	E	LV sub-epicardial	<1 min	8.2	Perpendicular
5	iii	F	LV mid-myocardial	<1 min	18.8	Perpendicular
6	iii	G	LV mid-myocardial	<1 min	6.5	Parallel
7	iii	H	LV sub-endocardial	~0.5 min	6.9	Perpendicular
8	iii	I	RV	<1 min	12.8	Not identified

were included the data analysis. Measurements in which data was distorted by external motion (e.g. gas bubbles breaking the fluid surface), or in which the pacing protocol failed to reliable capture the tissue at the desired frequency, were excluded.

2.6. Stretch protocol

After mounting a tissue slice onto the stretcher, a recovery period of 25–50 min was given to reach steady state. Stretch was applied manually, with amplitudes listed in Table 1 (note that the absolute amount of stretch varied, taking into account differences in the length of 'free tissue' between tissue attachment areas. Measurements of V_m and $[Ca^{2+}]_i$ were taken before, and shortly after stretch application (usually <1 min), and then every ~5–10 min, up to 50 min total duration (time intervals varied between preparations), to allow capture of dynamic changes in AP and CaT characteristics over time. Measurements were also taken shortly after release of stretch (<1 min). Fig. S1 in the online supplement shows a schematic of the stretch protocol.

Data analysed in this report is from 8 slices of 3 rabbits; one of the slices was stretched twice. In these proof-of-principle experiments, we used ventricular tissue from both LV and RV free wall (see Table 1 for overview).

For most slices, prevailing cell orientation (henceforth 'fibre direction') could be visually identified (Fig. 2A). Fibre direction was subsequently confirmed by light-microscopic scan after histologically processing (5 μm sections, Trichrome-stained; Fig. 2B). Although native tissue and histologically processed sections are not identical, this allows one to reconfirm the dominant fibre orientation, as this parameter does not rotate significantly over the thickness of the slice. For RV slices, we were unable to identify a single dominant fibre direction as cells were aligned more heterogeneously (stretch *vs.* cell alignment labelled as 'not identified' in Table 1).

2.7. Histological processing

After a slice was removed from the micromanipulator, it was sandwiched between a sponge and a glass coverslip, placed in a slotted tissue processing cassette, and fixed using the fast-acting Karnovsky's fixative (2% formaldehyde, 2.5% glutaraldehyde in cacodylate buffer, Solmedia Limited, Shrewsbury, UK). Tissue samples were stored in Karnovsky's until wax embedding. Wax-embedded tissue was cut into 5 μm thick sections using a rotary microtome (Leica RM2125; Milton Keynes, UK). These sections were then stained with Masson's trichrome. The protocol of wax embedding and Masson's trichrome staining has been described elsewhere (Plank et al., 2009). Stained sections were imaged (Fig. 2B) with a digital scanner (40× objective, Scanscope CS2, Aperio Ltd, Oxford, UK).

2.8. Data analysis

Data sets generated by optical mapping were analysed with an in-house semi-automatic data analysis tool (Wang et al., 2014) coded in Matlab® (The MathWorks; Natick, USA). Recorded signals (V_m and $[Ca^{2+}]_i$) were processed to reduce noise distortion before relevant parameters were extracted. For this study, we focus on investigating the influence of stretch on APD and CaT duration. APD80 and APD50 and CaT at 80% and 50% decay (CaT80 and CaT50, respectively) were analysed.

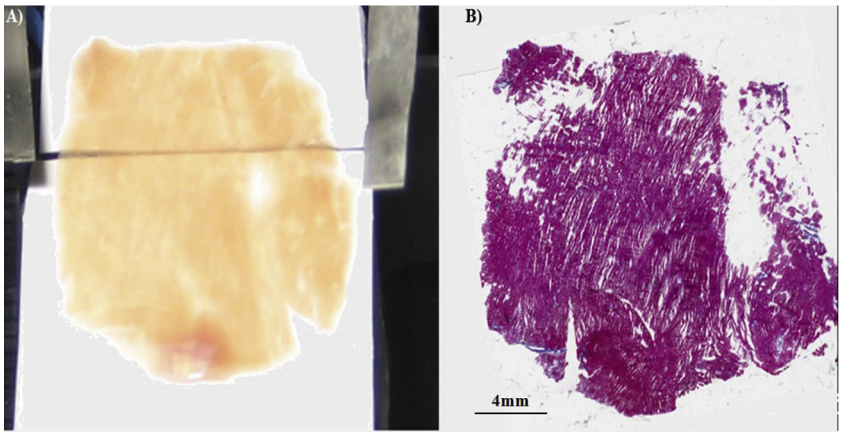

Fig. 2. LV mid-myocardial slice (preparation G) mounted for application of stretch in parallel to prevailing cell orientation. A) Photograph of the slice on the stretching device at control length. B) Digitized microscopy image of the same slice after fixation, sectioning at 5 μm thickness, and trichrome-staining.

For each pixel yielding a sufficiently strong fluorescent signal, APD and CaT were temporally averaged over 10 cardiac cycles to extract APD80, APD50, CaT80 and CaT50 for the location of that pixel. Maps and histograms based on these values were constructed (see Figs. 3–6). Mean and standard deviation (SD) values were calculated from the maps (e.g. mean APD80 shown in Fig. 3C). We did not exclude any parts of the map to avoid selection bias (i.e. the glued part of the tissue was not excluded, since there is no clearly identifiable 'contour' of the glued tissue in the fluorescent data). Pixels containing tissue with insufficient signal intensity are shown in grey in the parameter maps. APD80 and CaT80 were used instead of APD90 and CaT90 to reduce calculation error due to baseline noise. CaT amplitude was not analysed, as it was measured non-ratiometrically.

3. Results

3.1. Changes in AP after stretch

Both V_m and CaT were mapped before and during stretch, as well as after release. Steady-state APD and CaT durations before stretch (control) were compared with APD and CaT duration

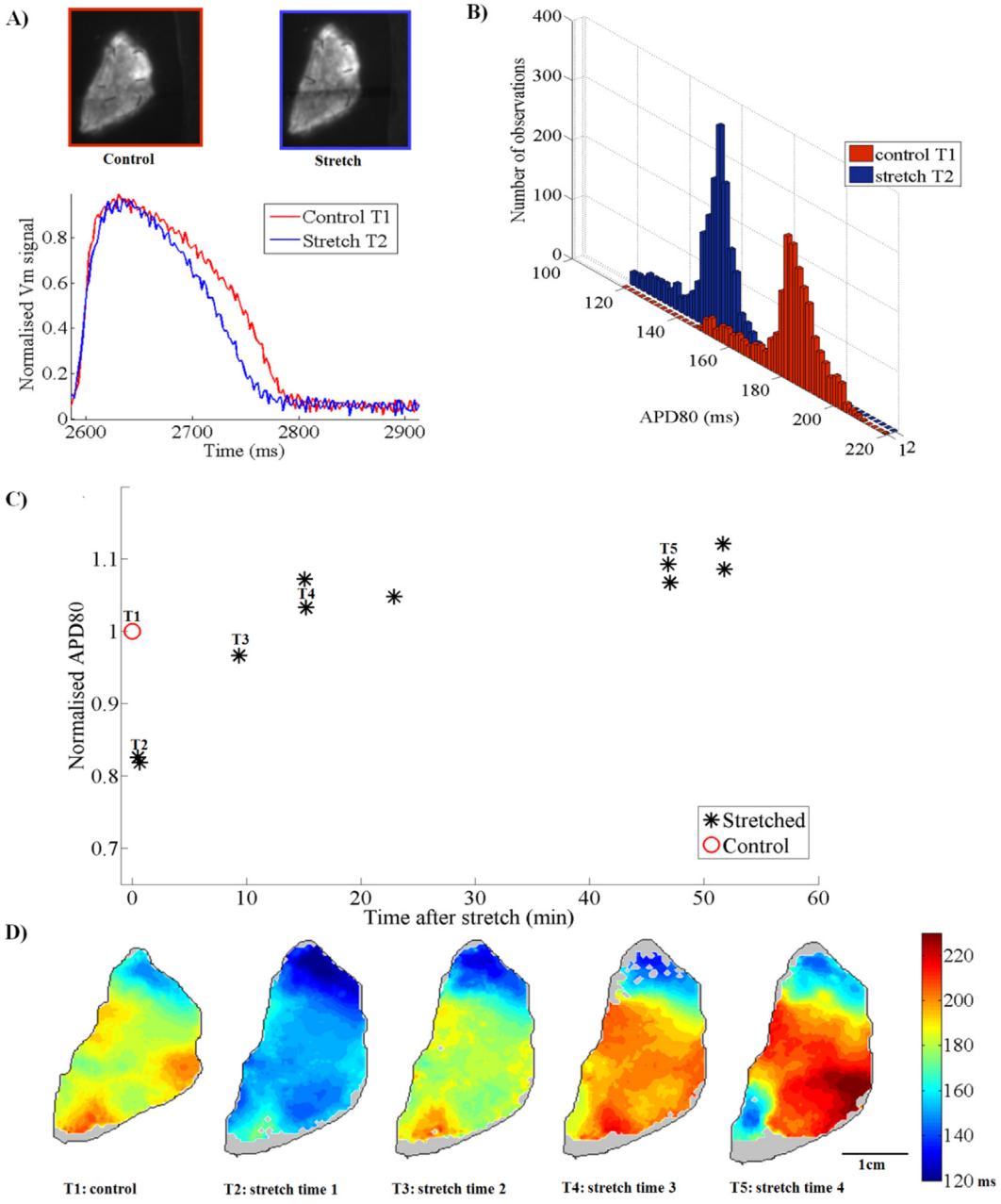

Fig. 3. Influence of stretch on the AP (preparation D in Table 1). A) Visible light images of the slice before and after application of stretch (top) and AP traces, averaged over the whole slice, before (red) and immediately after application of stretch (blue); B) Histogram of APD80, measured from the slice before (red) and immediately after application of stretch (blue); C) APD80, normalised to the control value (T1) at different time points after application of stretch; D) APD80 maps of this slice at 5 time points (T1 to T5 identified in subfigure C) show an initial stretch-induced decrease in APD80, followed by recovery and increase beyond control levels, in particular in the mid-are of the tissue, which would be maximally exposed to stretch (as opposed to the glued contact regions at the top and bottom of the slice, which will be less affected). Grey areas indicate tissue with insufficient fluorescent signal intensity (also in Figs. 4–6).

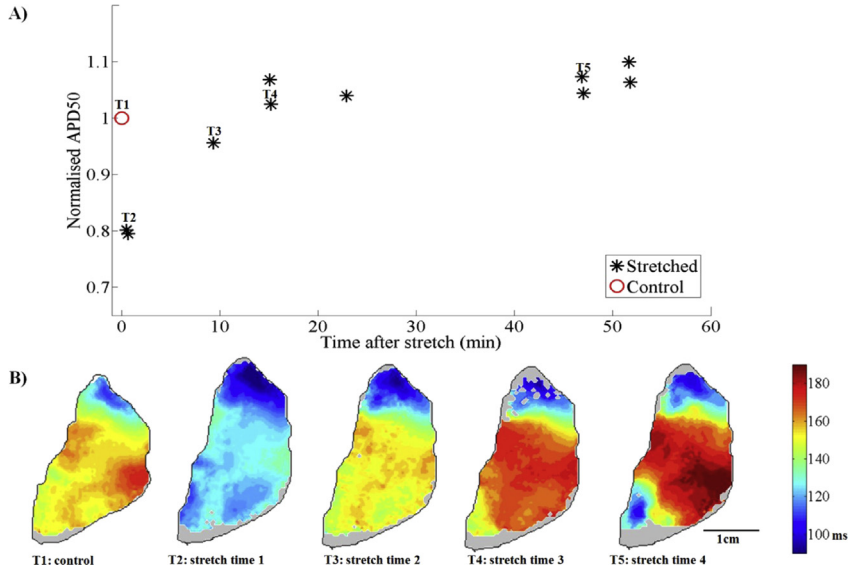

Fig. 4. Change in APD50 during stretch (preparation D in Table 1): A) APD50, normalised to the control value (T1), at different time points after stretch; B) APD50 map of this slice at 5 time points (T1 to T5, identified in subfigure A). As in Fig. 3, the initial drop in APD50 is followed by gradual increase beyond control values, present mainly in the central stretched part of the slice.

immediately after stretch (measured normally within less than one minute), and with subsequent changes occurring during sustained stretch (up to 50 min).

Fig. 3 contains an example of the data analysed. Fig. 3A shows the camera image of the slice before and after stretch, as well as the spatially averaged (over the whole slice) and normalised V_m trace from control and the first time point after application of stretch (here ~30 s), when APD shortening is observed. This shortening is present both at early (APD50) and late repolarisation (APD80). Fig. 3B shows a histogram of APD80 measured (over 10 cycles) before and immediately after application of stretch (note that the entire APD80 distribution shifts to lower values). A similar overall shortening immediately after application of stretch was seen for APD50 in all slices. APD80 and APD50 (see Table 2), observed in all 9 cases, were reduced by 10.7% and 11.4%, respectively. The averages shown in Table 2 (as well as in Tables 3–5) are spatially averaged values. Pair-wise *t*-test was preformed to assess whether there is a significant difference between APD (APD80 and APD50) immediately after stretch as compared to control (with the null hypothesis that the difference between control values and that immediately after stretch has a mean equal to zero). *P*-values of 0.001 and 0.002 were found for APD80 and APD50, respectively, indicating a significant difference (at 5% significant level) between pre-stretch controls and the value shortly after stretch.

To investigate whether further APD changes occur during maintained stretch, a series of measurements at different time points was taken (up to 50 min). In Fig. 3C, mean APD80 (normalised to control values) at different time points after stretch is shown. The pre-stretch control value (set to 1 as the reference value for the normalisation) is shown by a red circle, while the data points collected during stretch are indicated by black asterisks. After the initial reduction in APD80, a gradual increase is seen over time, approaching a new steady state, here with longer APD80 than in control. A similar pattern can be observed for APD50 (Fig. 4A, same slice). In Figs. 3D and 4B, maps of APD80 and APD50 are shown for five time points (T1 to T5, marked in the time-plot panels, with T1 = control, T2 = immediate response: ~30 s after application of stretch, and T3 to T5 = later time points during maintained stretch). The initial decrease in APD50 and APD80 over the whole slice after stretch (T2) is followed by gradual recovery from T2 to T5, yielding an increase in APD50 and APD80 compared to control. A similar response in APD50 and APD80 to stretch was seen in most slices; however the rate and amount of changes differed from case to case (see on-line Figs. S2 and S3).

3.2. Change in CaT after stretch

Results of stretch-induced changes in CaT duration are summarised in a similar fashion as APD. Fig. 5A shows the visible light image of a slice (same slice as in Figs. 3 and 4) before and after stretch (top), and the CaT trace, averaged over the whole slice. Fig. 5B shows the histogram of CaT80 distribution, measured before and immediately after application of stretch. A slight shortening of CaT80 and CaT50 (by 6.0%, and 5.3%, respectively), compared to control, can be observed (see also Fig. 6A). Table 3 summarises mean and SD of CaT80 and CaT50 before and immediately after application of stretch for the slices (CaT duration for preparations A and C are not shown as they did not yield a sufficient Ca^{2+} signal). Pair-wise *t*-test was also performed on CaT durations (CaT80 and CaT50) measured before and immediately after application of stretch. *P*-values of 0.001 and 0.003 were found for CaT80 and CaT50, respectively, indicating a significant difference (at 5% significant level). The shortening in CaT80 and CaT50 immediately after stretch is followed by gradual recovery, echoing APD changes, albeit with less pronounced relative amplitudes.

The initial reduction in CaT80 and CaT50 is followed by gradual recovery, occasionally exceeding control values. This is shown in Figs. 5C and 6A, where CaT80 and CaT50, normalised to the control value, are plotted at different time points. Figs. 5D and 6B show CaT80 and CaT50 maps at 5 time points (T1 = control, T2 = 30 s after application of stretch, T3–T5 = subsequent time points during stretch, as identified in Figs. 5C and 6A). Figs S4 and S5 in the online supplement summarise similar changes in CaT80 and CaT50 for most of the other slices.

3.3. Influence of stretch-release on APD and CaT

Upon release of stretch (measured within 1 min), both APD and CaT duration reversed to lower values, as summarised in Table 4 (APD) and Table 5 (CaT). The average shortening of the

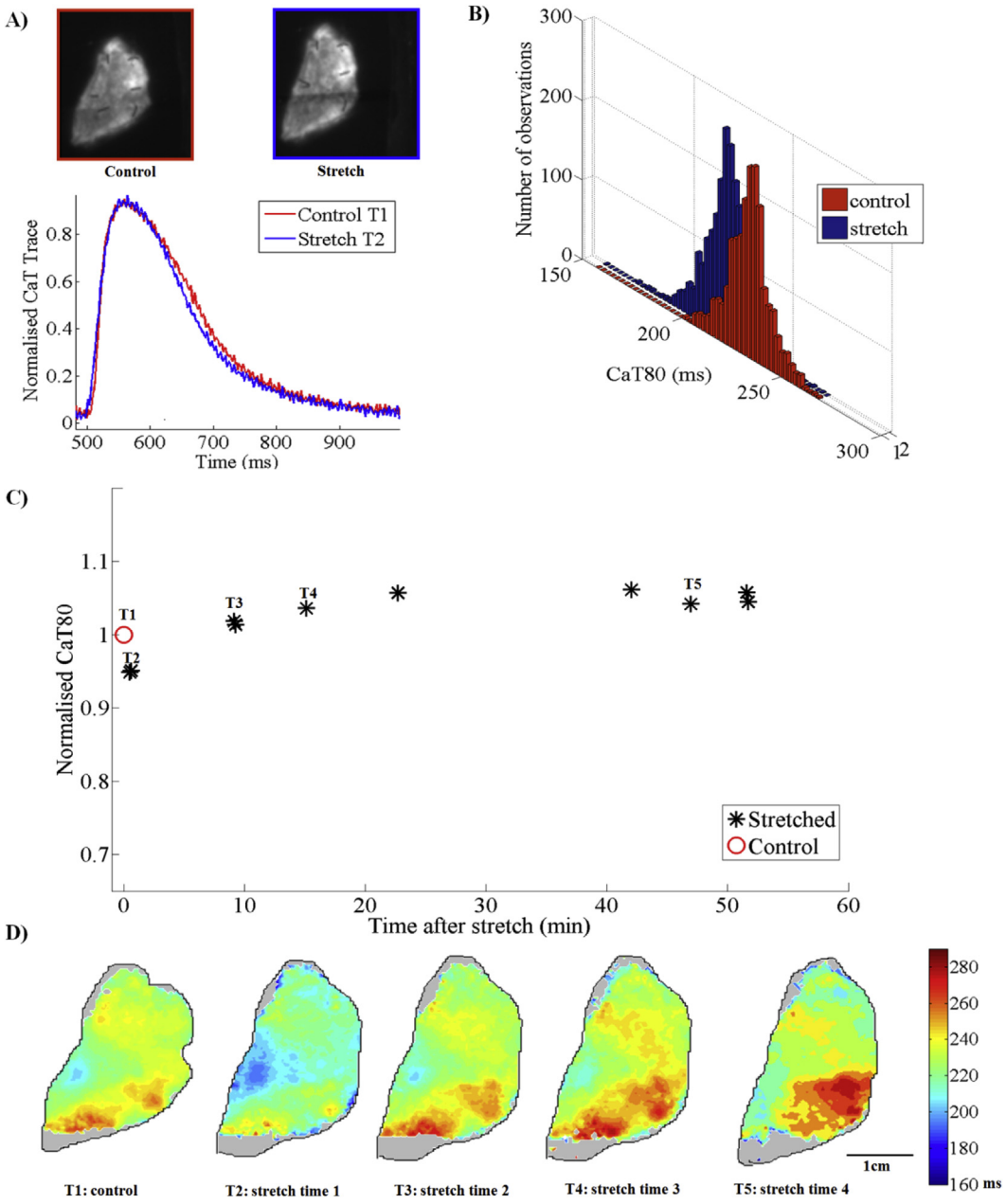

Fig. 5. Influence of stretch on CaT (preparation D in Table 1): A) visible light image of the slice before and after application of stretch (top) and plot of CaT traces, averaged over the whole slice, before (red) and immediately after application of stretch (blue); B) Histogram of CaT80 measured before (red) and immediately after application of stretch (blue); C) CaT80, normalised to control (T1) at different time points after stretch, showing a decrease in CaT80 immediately after stretch, followed by gradual recovery; D) CaT80 map of this slice at 5 different time points (T1 - T5, indicated in subfigure C).

(previously increased by sustained stretch) APD80 and APD50 were 6.7% and 7.9%, respectively. Pair-wise *t*-test performed on the APD (APD80 and APD50) measured shortly before and after releasing stretch show significant change (at 5% significant level) in both parameters (*P*-values: 0.004 and 0.002 respectively). For CaT duration, the decrease was more subtle, with an average shortening of CaT80 and CaT50 by 1.9% and 2.0%, respectively. Preparations A and B were excluded from analysis (see exclusion criteria in section 2.5); preparations C had a poor CaT signal and was excluded from Ca^{2+} analysis; CaT was not measured for preparation F after stretch-release. Significant differences in CaT durations (CaT80 and CaT50) measured before and shortly after releasing stretch were found with a pair-wise *t*-test (*P* values: 0.028 and 0.020 respectively).

4. Discussion

4.1. Transient stretch-induced reduction in APD and CaT duration

Data collected from rabbit ventricular tissue slices in this study show a decrease in both APD and CaT duration during the initial phase immediately following application of stretch (as shown in Figs. 3 and 4 and Table 2 for APD, and Figs. 5 and 6 and Table 3 for CaT).

Although the profiles of responses (amount of change, rate of recovery) in APD and CaT duration exhibit individual differences, the partial reversal of that reduction, i.e. a re-lengthening of both APD and CaT duration at subsequent time points, was generally

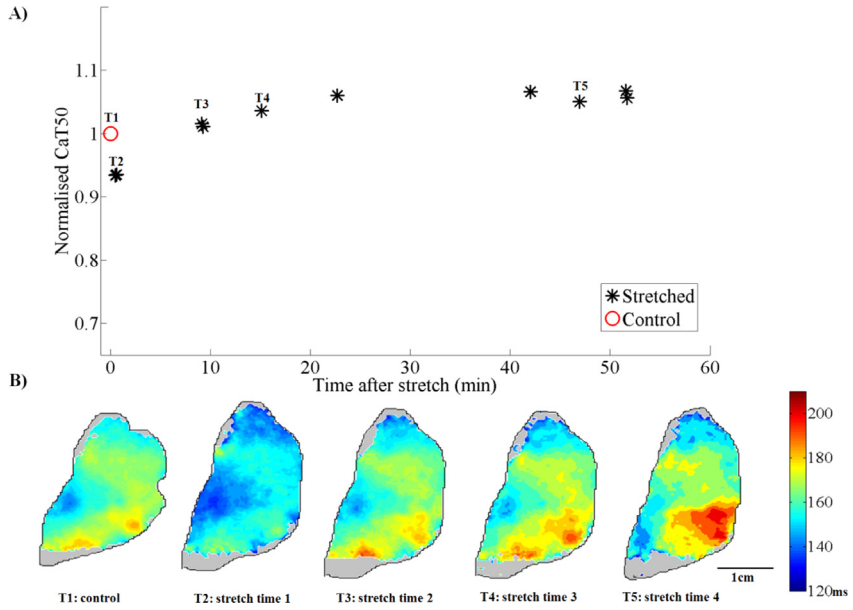

Fig. 6. Change of CaT50 during stretch (preparation D in Tab.): A) CaT50, normalised to control (T1) at different time points after application of stretch; B) CaT50 map of the slice at 5 different time points (T1 to T5, as marked in subfigure A) show initial decrease, followed by recovery in CaT50.

seen. In slices where new steady states in APD and CaT duration were reached, these could be longer than control values (e.g. Figs. 3 and 5). In the supplemental material, Figs. S2–S5 provide individual time lines for all slices.

These findings support the view that changes in APD and CaT duration during stretch are dynamic, while the acute response to stretch is shortening. This is in keeping with classic reports on the dynamic nature of both parameters, observed for APD (Allen, 1977) and CaT (Allen and Kurihara, 1982).

4.2. AP vs CaT

There is a qualitative correlation between the responses to stretch of APD and CaT duration, as described before (Kaufmann et al., 1971a), though the relative change in CaT duration is smaller than that of APD.

Stretch can co-affect both parameters through several mechanisms. Immediate SAC activation could drive the initial reduction in APD, with CaT following 'passively', while at later time points, the

Table 2
Comparison of APD80 and APD50 measured before (control) and immediately after stretch application (see Table 1 for timing information). Post-stretch values for both parameters differ significantly from control ($p \leq 0.002$).

Prep.	Control APD80 mean (ms)	Stretch APD80 mean (ms)	APD80 stretch/control %	Control APD50 mean (ms)	Stretch APD50 mean (ms)	APD50 stretch/control %
A	129.2 ± 14.1	126.9 ± 13.8	98.2	104.8 ± 13.3	103.2 ± 11.8	98.5
B	248.3 ± 28.4	195.5 ± 12.6	78.7	213.0 ± 36.0	166.6 ± 16.3	78.2
C	210.5 ± 15.5	182.2 ± 22.0	86.6	179.8 ± 16.6	152.1 ± 23.3	84.6
D	182.3 ± 11.4	150.5 ± 10.2	82.6	152.5 ± 12.3	122.2 ± 10.0	80.1
E	230.4 ± 25.1	213.1 ± 22.0	92.5	190.5 ± 26.3	176.6 ± 21.4	92.7
F	220.7 ± 19.8	203.6 ± 22.5	92.3	181.5 ± 27.3	168.1 ± 25.7	92.6
G	235.3 ± 19.3	216.7 ± 17.8	92.1	201.9 ± 19.5	185.2 ± 17.7	91.7
H	255.1 ± 42.4	219.5 ± 47.8	86.1	213.9 ± 46.3	179.2 ± 51.4	83.8
I	209.0 ± 38.9	197.0 ± 33.5	94.2	161.9 ± 43.4	154.1 ± 39.2	95.2
		Average	89.3		Average	88.6
		SD	6.2		SD	7.1

Table 3
Comparison of CaT80 and CaT50 measured before and immediately after application of stretch. Post-stretch values for both parameters differ significantly from control ($p \leq 0.004$).

Prep.	Control CaT80 mean (ms) ± SD	Stretch CaT80 mean (ms) ± SD	CaT80 stretch/control %	Control CaT50 mean (ms) ± SD	Stretch CaT50 mean (ms) ± SD	CaT50 stretch/control %
B	223.0 ± 18.0	199.3 ± 12.6	89.4	165.8 ± 15.4	151.6 ± 9.8	91.4
D	232.8 ± 11.1	218.1 ± 11.2	93.7	163.3 ± 8.0	150.6 ± 7.1	92.2
E	241.9 ± 20.3	235.1 ± 19.2	97.2	174.5 ± 15.6	171.1 ± 14.2	98.1
F	242.1 ± 15.6	226.3 ± 19.5	93.5	173.1 ± 12.5	163.3 ± 15.8	94.3
G	234.3 ± 19.3	216.7 ± 17.8	92.5	201.1 ± 19.5	185.2 ± 17.7	92.1
H	248.7 ± 24.9	235.3 ± 21.6	94.6	175.9 ± 18.8	171.0 ± 18.2	97.2
I	244.6 ± 22.6	237.4 ± 20.7	97.1	177.7 ± 21.9	173.7 ± 19.0	97.8
		Average	94.0			94.7
		SD	2.7			2.9

Table 4
Comparison of APD80 measured before and immediately after stretch-release. Post-release values for both parameters differ significantly from pre-release values ($p \leq 0.004$).

Prep.	Stretch APD80 mean (ms) ± SD	Release APD80 mean (ms) ± SD	APD80 release/stretch %	Stretch APD50 mean (ms) ± SD	Release APD50 mean (ms) ± SD	APD50 release/stretch %
C	187.2 ± 24.9	181.1 ± 21.9	96.7	154.0 ± 26.0	148.2 ± 23.4	96.2
D	201.2 ± 23.0	178.9 ± 19.9	88.9	164.8 ± 25.6	144.3 ± 22.5	87.5
E	213.1 ± 22.0	202.5 ± 17.5	95.0	176.6 ± 21.4	165.8 ± 17.7	93.9
F	217.5 ± 36.3	212.6 ± 29.9	97.7	180.0 ± 36.7	171.4 ± 34.0	95.2
G	229.6 ± 37.9	221.7 ± 38.1	96.6	187.5 ± 48.2	179.5 ± 45.9	95.7
H	189.5 ± 73.0	172.8 ± 65.6	91.2	150.2 ± 70.4	136.3 ± 63.8	90.8
I	217.6 ± 34.2	189.9 ± 34.0	87.3	174.3 ± 39.7	148.6 ± 35.6	85.3
		Average	93.3		Average	92.1
		SD	4.2		SD	4.3

increased CaT that is associated with the slow force response (von Lewinski et al., 2005) could drive the recovery of APD.

An alternative explanation for the transient nature of stretch-induced reductions in APD and CaT duration is partial tissue recovery, by re-lengthening of viscous elements (Kohl et al., 1999). This could reduce the mechanical stimulus, effective at the cellular level, and should be monitored in future (for example using fluorescent beads on the slice surface to assess regional strain patterns).

To explore the interplay, between V_m and CaT, simultaneous V_m and $[Ca^{2+}]_i$ mapping would be a valuable extension. This is a relatively easy add-on to the here presented set-up, for example using the approach by Lee et al. (2012). Also, alternative interventions targeting either SAC or Ca^{2+} handling to perturb the system (e.g. via pharmacological manipulation) may help in revealing more of the mechanisms underlying the dynamic APD and CaT duration responses to stretch.

4.3. Stretch-release

Similar to the contradictory observations on stretch-induced changes in APD and CaT duration, the effects of stretch-release are debated. They, too, appear to depend on time of observation, contractile state of the tissue, amplitude and dynamics of re-shortening, and other experimental environment parameters (Hennekes et al., 1977; Lab, 1980, 1982). Our measurements show that APD decreased right after release of stretch, which is in keeping with data published by Sung et al. (2003). Assuming that the moderate prolongation of APD and CaT duration after the initial stretch-induced drop was related to a slow force response mechanism, it is reasonable to expect that after termination of the stretch, APD and CaT duration could return to their initial control value, as described by Lab (Lab, 1980). This would be expected to occur over roughly the same period of time as slow force response development during stretch, thus identifying an additional target for further research. Again, changes in APD are more pronounced than those in CaT duration (Tables 4 and 5). It would be interesting to investigate their dynamics over a longer period of time after stretch-release, to capture long-term and steady-state effects.

4.4. Utility of living tissue slices as a model for cardiac MEF research

Cardiac tissue slices with their locally preserved cell–cell connections and cell-type distribution (including both myocytes and non-myocytes) combine moderate complexity with the potential for effective experimental control (input) and observation (output). Of note, they are amenable to use on human cardiac tissue (Camelliti et al., 2011; Brandenburger et al., 2012). Compared to whole heart, although the electrical coupling in the third dimension is severely reduced, and extracellular spaces are less preserved (Anyukhovsky et al., 1999), this reduced complexity can be beneficial. Thus, electrical activation, for example, occurs in a much simpler fashion, allowing better control over pacing rate and site, and directionality of conduction. As an experimental model system, slices also offer the opportunity to collect multiple tissue samples, and tissue from different regions, of one heart (e.g. LV free wall *vs.* RV free wall; sub-epicaridal, mid-myocaridal or sub-endocardial layers) allowing multiple experimental investigations from the same sample, and exploration of regional difference in behaviour. Although we did not explore this aspect in detail here, we show that it is possible to collect multiple slices with decent V_m and CaT signal from various transmural layers of LV tissue, and of the RV, from one and the same heart.

Tissue slices have been used acutely for up to 8–9 h after sectioning (Burnashev et al., 1990; Camelliti et al., 2011) and have also been used after weeks' of culturing (Brandenburger et al., 2012). All our experiments were conducted within a time window of 5 h. This is a period during which maintained ultrastructural integrity has been confirmed for the protocols used here (Wang et al., 2014).

Since the dominant fibre direction in tangentially cut (parallel to epicardial plane) cardiac tissue slices can, in most cases, be identified with ease, stretch can be applied in principle using the dominant fibre direction as a reference (e.g. perpendicular, parallel, or at any desired angle relative to fibre orientation). This allows investigation of potential difference between stretch effects on cells depending on their orientation relative to the main direction of stretch.

Table 5
Comparison of CaT80 and CaT50 before and immediately after stretch-release Post-release values for both parameters differ significantly from pre-release values ($p \leq 0.03$).

Prep.	Stretch CaT80 mean (ms) ± SD	Release CaT80 mean (ms) ± SD	CaT80 release/stretch/%	Stretch CaT50 mean (ms) ± SD	Release CaT50 mean (ms) ± SD	CaT50 release/stretch %
D	243.2 ± 15.8	234.3 ± 16.2	96.3	172.2 ± 13.5	165.1 ± 13.0	95.9
E	237.4 ± 18.8	234.2 ± 19.1	98.7	172.4 ± 13.3	169.5 ± 13.9	98.3
G	231.8 ± 15.0	230.3 ± 14.7	99.3	166.8 ± 12.6	165.2 ± 13.1	99.1
H	216.6 ± 35.8	212.5 ± 33.4	98.1	154.1 ± 29.6	151.7 ± 28.8	98.5
I	245.2 ± 21.4	241.1 ± 20.2	98.3	180.8 ± 19.1	177.6 ± 18.4	98.2
		Average	98.1		Average	98.0
		SD	1.1		SD	1.2

Although the cutting of cardiac tissue slices in parallel to the epicardial plane yields sections with a high proportion of in-plane fibres (Yasuhara et al., 1996; Bussek et al., 2009), this orderly alignment becomes less pronounced as one approaches sub-endocardial layers. When point stimulation is used to pace slices with clear fibre direction, a conduction map showing pronounced anisotropy can be captured. With algorithm such as developed by Bayly et al. (1998), conduction velocities can be estimated for each point. This makes it potentially easy to capture conduction velocity changes during and after stretch. However, conduction from point-stimulation sites is affected by uneven source-sink distribution, and this can yield contradictory results in one and the same tissue slice, depending on stimulation site (Wang et al., 2014). For this reason, we focussed our analysis here on field stimulation. The use of point stimulation to capture conduction velocity changes during and/or after stretch (Dominguez and Fozzard, 1979; Zhang et al., 2008) is an interesting topic for further study in cardiac slices.

4.5. Utility of optical mapping

Electrophysiological behaviour of cardiac tissue slices has mainly been explored using multi-electrode arrays (Bussek et al., 2009). These monitor V_m without capturing AP shape, and at relatively low spatial resolution. Optical mapping addresses these limitations, and allows one to extend the study of MEF to other parameters, such as $[Ca^{2+}]_i$, and hence to capture two highly relevant parameters for cardiac electro-mechanics research.

Optical mapping can be also combined with motion/deformation tracking, for example using structured light (Laughner et al., 2012) or fluorescent beads (McCulloch et al., 2005). This can provide information about local slice deformation, including acute and possible delayed effects (e.g. viscous re-lengthening). This data would be useful for assessing the homogeneity (or lack thereof) of stretch effects on the tissue, and for a more careful interrelation of local stretch, APD and CaT changes.

4.6. Study limitations

This study was a proof-of-principle attempt to investigate the utility of living cardiac tissue slices as an experimental model for MEF studies, involving optical mapping of both V_m and $[Ca^{2+}]_i$. In addition to the outlined benefits, above, our experiments identified several limitations with the current methodology.

i) Amount, timing and speed of stretch may influence effects on APD and CaT duration (Le Guennec et al., 1991; Zabel et al., 1996; Nishimura et al., 2006); this study was not designed to investigate their influences. To do so, the manual stretcher should be replaced by a computer-controlled motorised device, to improve spatial and temporal control over the intervention.
ii) Monitoring of local deformation should be added, to allow correlation of local changes in mechanics, electrics, and ion handling.
iii) CaT amplitude is an important parameter that is known to be affected by maintained stretch. This can be studied, using ratiometric Ca^{2+} measurements. A dual and ratiometric V_m/Ca^{2+} mapping system has been developed (Lee et al., 2011), and will be used in future studies. In this context, it is important to note that the Ca^{2+} sensitive dye used (Rhod-2) has a relatively high affinity for Ca^{2+}. High affinity dyes may suffer from saturation (Woods et al., 2004), and therefore would not capture real CaT peak amplitudes. The ratiometric studies proposed above should therefore include a low-affinity Ca^{2+} dye (e.g. Rhod-ff), or use two dyes (e.g. Rhod-2 and Rhod-ff) for comparison.
iv) The use of tissue glue has several advantages: it can be used to mount tissue onto the stretcher, regardless of slice shape, it acts quickly, holds the slice down relatively strongly, and does not give rise to foci of excess point deformation (as, for example, pins would). However, there are disadvantages, as the glue may influence the vitality of the tissue, in particular where glue is applied (limited perfusion/access to oxygen). Also, in spite of all efforts, it cannot be excluded that during the attachment process, slices are exposed to mechanical deformation or pre-stretch. Finally, once glued down, correction of slice position or rotation is not possible without high risk for tissue damage.

5. Conclusions

Living cardiac tissue slices constitute a 2D organotypic model of myocardium, which can be combined successfully with multi-parametric optical mapping, and used to investigate the effects of axial stretch on V_m and CaT. Their use opens up new possibilities for the study of cardiac biophysics in general, and the dynamic interrelations of cardiac structure, mechanics, and electrics in particular.

Editors' note

Please see also related communications in this issue by Solovyova et al. (2014) and Iribe et al. (2014).

Acknowledgement

This work was supported by the Qatar Foundation (CB), the British Heart Foundation (BHF; grants to PK), the Magdi Yacoub Institute (CB, PK), and ERC Advanced Grant CardioNect (PK). We further gratefully acknowledge a Microsoft Research fellowship to KW. PK is a Senior Fellow of the BHF. We further thank Prof Stefan Luther for providing the PVCAM recording software, Prof Leslie M. Loew for access to voltage-sensitive dyes, and Dr Padmini Sarathchandra for help with and advice on histology.

Appendix A. Supplementary data

Supplementary data related to this article can be found at 10.1016/j.pbiomolbio.2014.08.006.

References

Allen, D.G., 1975. The Variations in Contractility of Cardiac Muscle. Ph.D. thesis. University of London.
Allen, D.G., 1977. On the relationship between action potential duration and tension in cat papillary muscle. Cardiovasc Res. 11, 210–218.
Allen, D.G., Kentish, J.C., 1988. Calcium concentration in the myoplasm of skinned ferret ventricular muscle following changes in muscle length. J. Physiol. 407, 489–503.
Allen, D.G., Kurihara, S., 1982. The effects of muscle length on intracellular calcium transients in mammalian cardiac muscle. J. Physiol. 327, 79–94.
Alvarez, B.V., Perez, N.G., Ennis, I.L., Camilion de Hurtado, M.C., Cingolani, H.E., 1999. Mechanisms underlying the increase in force and Ca^{2+} transient that follow stretch of cardiac muscle: a possible explanation of the Anrep effect. Circ. Res. 85, 716–722.
Anyukhovsky, E.P., Sosunov, E.A., Gainullin, R.Z., Rosen, M.R., 1999. The controversial M cell. J. Cardiovasc Electrophysiol. 10, 244–260.
Baumgarten, C.M., 2000. Origin of Mechanotransduction: Stretch-activated Ion Channels. Madame Curie Bioscience Database Landes Bioscience, Austin (TX).
Baumgarten, C.M., Clemo, H.F., 2003. Swelling-activated chloride channels in cardiac physiology and pathophysiology. Prog. Biophys. Mol. Biol. 82, 25–42.
Bayly, P.V., KenKnight, B.H., Rogers, J.M., Hillsley, R.E., Ideker, R.E., Smith, W.M., 1998. Estimation of conduction velocity vector fields from epicardial mapping data. IEEE Trans. Biomed. Eng. 45, 563–571.

Belmonte, S., Morad, M., 2008a. 'Pressure-flow'-triggered intracellular Ca^{2+} transients in rat cardiac myocytes: possible mechanisms and role of mitochondria. J. Physiol. 586, 1379–1397.

Belmonte, S., Morad, M., 2008b. Shear fluid-induced Ca^{2+} release and the role of mitochondria in rat cardiac myocytes. Ann. N. Y. Acad. Sci. 1123, 58–63.

Belus, A., White, E., 2003. Streptomycin and intracellular calcium modulate the response of single guinea-pig ventricular myocytes to axial stretch. J. Physiol. 546, 501–509.

Bollensdorff, C., Lookin, O., Kohl, P., 2011. Assessment of contractility in intact ventricular cardiomyocytes using the dimensionless 'Frank-Starling Gain' index. Pflugers Arch. 462, 39–48.

Botchway, A.N., Turner, M.A., Sheridan, D.J., Flores, N.A., Fry, C.H., 2003. Electrophysiological effects accompanying regression of left ventricular hypertrophy. Cardiovasc Res. 60, 510–517.

Brandenburger, M., Wenzel, J., Bogdan, R., Richardt, D., Nguemo, F., Reppel, M., Hescheler, J., Terlau, H., Dendorfer, A., 2012. Organotypic slice culture from human adult ventricular myocardium. Cardiovasc Res. 93, 50–59.

Burnashev, N.A., Edwards, F.A., Verkhratsky, A.N., 1990. Patch-clamp recordings on rat cardiac muscle slices. Pflugers Arch. 417, 123–125.

Bussek, A., Wettwer, E., Christ, T., Lohmann, H., Camelliti, P., Ravens, U., 2009. Tissue slices from adult mammalian hearts as a model for pharmacological drug testing. Cell. Physiol. Biochem 24, 527–536.

Bustamante, J.O., Ruknudin, A., Sachs, F., 1991. Stretch-activated channels in heart cells: relevance to cardiac hypertrophy. J. Cardiovasc Pharmacol. 17 (Suppl. 2), S110–S113.

Calaghan, S.C., Belus, A., White, E., 2003. Do stretch-induced changes in intracellular calcium modify the electrical activity of cardiac muscle? Prog. Biophys. Mol. Biol. 82, 81–95.

Caldwell, R.A., Clemo, H.F., Baumgarten, C.M., 1998. Using gadolinium to identify stretch-activated channels: technical considerations. Am. J. Physiol. 275, C619–C621.

Camelliti, P., Al-Saud, S.A., Smolenski, R.T., Al-Ayoubi, S., Bussek, A., Wettwer, E., Banner, N.R., Bowles, C.T., Yacoub, M.H., Terracciano, C.M., 2011. Adult human heart slices are a multicellular system suitable for electrophysiological and pharmacological studies. J. Mol. Cell. Cardiol. 51, 390–398.

Camelliti, P., Gallagher, J.O., Kohl, P., McCulloch, A.D., 2006. Micropatterned cell cultures on elastic membranes as an in vitro model of myocardium. Nat. Protoc. 1, 1379–1391.

Camelliti, P., Green, C.R., LeGrice, I., Kohl, P., 2004. Fibroblast network in rabbit sinoatrial node: structural and functional identification of homogeneous and heterogeneous cell coupling. Circ. Res. 94, 828–835.

Cooper, P.J., Epstein, A., Macleod, I.A., Schaaf, S.T., Sheldon, J., Boulin, C., Kohl, P., 2006. Soft tissue impact characterisation kit (STICK) for ex situ investigation of heart rhythm responses to acute mechanical stimulation. Prog. Biophys. Mol. Biol. 90, 444–468.

Cooper, P.J., Kohl, P., 2005. Species- and preparation-dependence of stretch effects on sino-atrial node pacemaking. Ann. N. Y. Acad. Sci. 1047, 324–335.

Cooper, P.J., Lei, M., Cheng, L.X., Kohl, P., 2000. Selected contribution: axial stretch increases spontaneous pacemaker activity in rabbit isolated sinoatrial node cells. J. Appl. Physiol. (1985) 89, 2099–2104.

Craelius, W., Chen, V., el-Sherif, N., 1988. Stretch activated ion channels in ventricular myocytes. Biosci. Rep. 8, 407–414.

de Boer, T.P., Camelliti, P., Ravens, U., Kohl, P., 2009. Myocardial tissue slices: organotypic pseudo-2D models for cardiac research & development. Future Cardiol. 5, 425–430.

Di Virgilio, F., Steinberg, T.H., Silverstein, S.C., 1990. Inhibition of Fura-2 sequestration and secretion with organic anion transport blockers. Cell. Calcium 11, 57–62.

Dominguez, G., Fozzard, H.A., 1979. Effect of stretch on conduction velocity and cable properties of cardiac Purkinje fibers. Am. J. Physiol. 237, C119–C124.

duBell, W.H., Boyett, M.R., Spurgeon, H.A., Talo, A., Stern, M.D., Lakatta, E.G., 1991. The cytosolic calcium transient modulates the action potential of rat ventricular myocytes. J. Physiol. 436, 347–369.

Eckardt, L., Kirchhof, P., Breithardt, G., Haverkamp, W., 2001. Load-induced changes in repolarization: evidence from experimental and clinical data. Basic Res. Cardiol. 96, 369–380.

Franz, M.R., Burkhoff, D., Yue, D.T., Sagawa, K., 1989. Mechanically induced action potential changes and arrhythmia in isolated and in situ canine hearts. Cardiovasc Res. 23, 213–223.

Gannier, F., White, E., Garnier, Le Guennec, J.Y., 1996. A possible mechanism for large stretch-induced increase in $[Ca^{2+}]_i$ in isolated guinea-pig ventricular myocytes. Cardiovasc. Res. 32, 158–167.

Gannier, F., White, E., Lacampagne, A., Garnier, D., Le Guennec, J.Y., 1994. Streptomycin reverses a large stretch induced increases in $[Ca^{2+}]_i$ in isolated guinea pig ventricular myocytes. Cardiovasc Res. 28, 1193–1198.

Garny, A., Noble, D., Kohl, P., 2005. Dimensionality in cardiac modelling. Prog. Biophys. Mol. Biol. 87, 47–66.

Gopalan, S.M., Flaim, C., Bhatia, S.N., Hoshijima, M., Knoell, R., Chien, K.R., Omens, J.H., McCulloch, A.D., 2003. Anisotropic stretch-induced hypertrophy in neonatal ventricular myocytes micropatterned on deformable elastomers. Biotechnol. Bioeng. 81, 578–587.

Guharay, F., Sachs, F., 1984. Stretch-activated single ion channel currents in tissue-cultured embryonic chick skeletal muscle. J. Physiol. 352, 685–701.

Healy, S.N., McCulloch, A.D., 2005. An ionic model of stretch-activated and stretch-modulated currents in rabbit ventricular myocytes. Europace 7 (Suppl. 2), 128–134.

Hennekes, R., Kaufmann, R., Lab, M., Steiner, R., 1977. Feedback loops involved in cardiac excitation-contraction coupling: evidence for two different pathways. J. Mol. Cell. Cardiol. 9, 699–713.

Hongo, K., White, E., Le Guennec, J.Y., Orchard, C.H., 1996. Changes in $[Ca^{2+}]_i$, $[Na^+]_i$ and Ca^{2+} current in isolated rat ventricular myocytes following an increase in cell length. J. Physiol. 491 (Pt 3), 609–619.

Hu, H., Sachs, F., 1997. Stretch-activated ion channels in the heart. J. Mol. Cell. Cardiol. 29, 1511–1523.

Iribe, G., Helmes, M., Kohl, P., 2007. Force-length relations in isolated intact cardiomyocytes subjected to dynamic changes in mechanical load. Am. J. Physiol. Heart Circ. Physiol. 292, H1487–H1497.

Iribe, G., Kohl, P., 2008. Axial stretch enhances sarcoplasmic reticulum Ca^{2+} leak and cellular Ca^{2+} reuptake in guinea pig ventricular myocytes: experiments and models. Prog. Biophys. Mol. Biol. 97, 298–311.

Iribe, G., Ward, C.W., Camelliti, P., Bollensdorff, C., Mason, F., Burton, R.A., Garny, A., Morphew, M.K., Hoenger, A., Lederer, W.J., Kohl, P., 2009. Axial stretch of rat single ventricular cardiomyocytes causes an acute and transient increase in Ca^{2+} spark rate. Circ. Res. 104, 787–795.

Iribe, G., Kaneko, T., Yamaguchi, Y., Naruse, K., 2014. Load dependency in force-length relations in isolated single cardiomyocytes. Prog. Bio. Mol. Biol. 115 (2-3), 103–114. http://dx.doi.org/10.1016/j.pbiomolbio.2014.06.005.

Isenberg, G., Kazanski, V., Kondratev, D., Gallitelli, M.F., Kiseleva, I., Kamkin, A., 2003. Differential effects of stretch and compression on membrane currents and $[Na^+]c$ in ventricular myocytes. Prog. Biophys. Mol. Biol. 82, 43–56.

Isenberg, G., Kondratev, D., Dyachenko, V., Kazanski, V., Gallitelli, M.F., 2005. Isolated cardiomyocytes: mechanosensitivity of action potential, membrane current and ion concentration. In: Kamkin, A., Kiseleva, I. (Eds.), Mechanosensitivity in Cells and Tissues. Moscow.

Janvier, N.C., Boyett, M.R., 1996. The role of Na–Ca exchange current in the cardiac action potential. Cardiovasc. Res. 32, 69–84.

Kamkin, A., Kirischuk, S., Kiseleva, I., 2010. Single mechano-gated channels activated by mechanical deformation of acutely isolated cardiac fibroblasts from rats. Acta Physiol. (Oxf) 199, 277–292.

Kamkin, A., Kiseleva, I., Isenberg, G., 2000. Stretch-activated currents in ventricular myocytes: amplitude and arrhythmogenic effects increase with hypertrophy. Cardiovasc Res. 48, 409–420.

Kaufmann, R.L., Antoni, H., Hennekes, R., Jacob, R., Kohlhardt, M., Lab, M.J., 1971a. Mechanical response of the mammalian myocardium to modifications of the action potential. Cardiovasc. Res.. Suppl. 1, 64–70.

Kaufmann, R.L., Lab, M.J., Hennekes, R., Krause, H., 1971b. Feedback interaction of mechanical and electrical events in the isolated mammalian ventricular myocardium (cat papillary muscle). Pflugers Arch. 324, 100–123.

Kim, D., 1992. A mechanosensitive K^+ channel in heart cells. Activation by arachidonic acid. J. Gen. Physiol. 100, 1021–1040.

Kiseleva, I., Kamkin, A., Kohl, P., Lab, M.J., 1996. Calcium and mechanically induced potentials in fibroblasts of rat atrium. Cardiovasc Res. 32, 98–111.

Kohl, P., Bollensdorff, C., Garny, A., 2006. Effects of mechanosensitive ion channels on ventricular electrophysiology: experimental and theoretical models. Exp. Physiol. 91, 307–321.

Kohl, P., Bollensdorff, C., Morad, M., 2012. Progress in biophysics and molecular biology of the beating heart. Prog. Biophys. Mol. Biol. 110, 151–153.

Kohl, P., Day, K., Noble, D., 1998. Cellular mechanisms of cardiac mechano-electric feedback in a mathematical model. Can. J. Cardiol. 14, 111–119.

Kohl, P., Gourdie, R.G., 2014. Fibroblast-myocyte electrotonic coupling: does it occur in native cardiac tissue? J. Mol. Cell. Cardiol. 70, 37–46.

Kohl, P., Hunter, P., Noble, D., 1999. Stretch-induced changes in heart rate and rhythm: clinical observations, experiments and mathematical models. Prog. Biophys. Mol. Biol. 71, 91–138.

Kohl, P., Nesbitt, A.D., Cooper, P.J., Lei, M., 2001. Sudden cardiac death by Commotio cordis: role of mechano-electric feedback. Cardiovasc. Res. 50, 280–289.

Kohl, P., Sachs, F., 2001. Mechanoelectric feedback in cardiac cells. Phil. Trans. R. Soc. 359, 1173–1185.

Kong, C.R., Bursac, N., Tung, L., 2005. Mechanoelectrical excitation by fluid jets in monolayers of cultured cardiac myocytes. J. Appl. Physiol. (1985) 98, 2328–2336. Discussion 2320.

Konishi, M., Berlin, J.R., 1993. Ca transients in cardiac myocytes measured with a low affinity fluorescent indicator, furaptra. Biophys. J. 64, 1331–1343.

Lab, M.J., 1978. Mechanically dependent changes in action potentials recorded from the intact frog ventricle. Circ. Res. 42, 519–528.

Lab, M.J., 1980. Transient depolarisation and action potential alterations following mechanical changes in isolated myocardium. Cardiovasc. Res. 14, 624–637.

Lab, M.J., 1982. Contraction-excitation feedback in myocardium. Physiological basis and clinical relevance. Circ. Res. 50, 757–766.

Lab, M.J., 1996. Mechanoelectric feedback (transduction) in heart: concepts and implications. Cardiovasc Res. 32, 3–14.

Lab, M.J., 1999. Mechanosensitivity as an integrative system in heart: an audit. Prog. Biophys. Mol. Biol. 71, 7–27.

Langendorff, O., 1895. Untersuchungen am uberlebenden Saugethierherzen. Pflügers Arch. 61, 291–332.

Laughner, J.I., Zhang, S., Li, H., Shao, C.C., Efimov, I.R., 2012. Mapping cardiac surface mechanics with structured light imaging. Am. J. Physiol. Heart Circ. Physiol. 303, H712–H720.

Le Guennec, J.Y., Peineau, N., Argibay, J.A., Mongo, K.G., Garnier, D., 1990. A new method of attachment of isolated mammalian ventricular myocytes for tension

recording: length dependence of passive and active tension. J. Mol. Cell. Cardiol. 22, 1083–1093.
Le Guennec, J.Y., White, E., Gannier, F., Argibay, J.A., Garnier, D., 1991. Stretch-induced increase of resting intracellular calcium concentration in single guinea-pig ventricular myocytes. Exp. Physiol. 76, 975–978.
Lee, K.S., Marban, E., Tsien, R.W., 1985. Inactivation of calcium channels in mammalian heart cells: joint dependence on membrane potential and intracellular calcium. J. Physiol. 364, 395–411.
Lee, P., Bollensdorff, C., Quinn, T.A., Wuskell, J.P., Loew, L.M., Kohl, P., 2011. Single-sensor system for spatially resolved, continuous, and multiparametric optical mapping of cardiac tissue. Heart Rhythm 8, 1482–1491.
Lee, P., Wang, K., Woods, C.E., Yan, P., Kohl, P., Ewart, P., Loew, L.M., Terrar, D.A., Bollensdorff, C., 2012. Cardiac electrophysiological imaging systems scalable for high-throughput drug testing. Pflugers Arch. 464, 645–656.
Lerman, B.B., Burkhoff, D., Yue, D.T., Franz, M.R., Sagawa, K., 1985. Mechanoelectrical feedback: independent role of preload and contractility in modulation of canine ventricular excitability. J. Clin. Invest 76, 1843–1850.
Lerman, B.B., Engelstein, E.D., Burkhoff, D., 2001. Mechanoelectrical feedback: role of beta-adrenergic receptor activation in mediating load-dependent shortening of ventricular action potential and refractoriness. Circulation 104, 486–490.
Madias, C., Maron, B.J., Alsheikh-Ali, A.A., Rajab, M., Estes 3rd, N.A., Link, M.S., 2009. Precordial thump for cardiac arrest is effective for asystole but not for ventricular fibrillation. Heart Rhythm 6, 1495–1500.
Markhasin, V.S., Balakin, A.A., Katsnelson, L.B., Konovalov, P., Lookin, O.N., Protsenko, Y., Solovyova, O., 2012. Slow force response and auto-regulation of contractility in heterogeneous myocardium. Prog. Biophys. Mol. Biol. 110, 305–318.
Markhasin, V.S., Solovyova, O., Katsnelson, L.B., Protsenko, Y., Kohl, P., Noble, D., 2003. Mechano-electric interactions in heterogeneous myocardium: development of fundamental experimental and theoretical models. Prog. Biophys. Mol. Biol. 82, 207–220.
Maron, B.J., Gohman, T.E., Kyle, S.B., Estes 3rd, N.A., Link, M.S., 2002. Clinical profile and spectrum of commotio cordis. JAMA 287, 1142–1146.
McCulloch, A.D., Gallagher, J.O., Bhatia, S.N., Borg, T.K., Omens, J.H., 2005. Three-dimensional micropatterned cardiac tissue cultures. Microsc. Microanal. 11, 110–111.
McCulloch, A.D., Pfeiffer, E., Tangney, J., Omens, J., 2013. Biomechanics of cardiac electromechanical coupling and mechanoelectric feedback. J. Biomech. Eng..
Moss, R.L., Fitzsimons, D.P., 2002. Frank-Starling relationship: long on importance, short on mechanism. Circ. Res. 90, 11–13.
Nakagawa, A., Arita, M., Shimada, T., Shirabe, J., 1988. Effects of mechanical stretch on the membrane potential of guinea pig ventricular muscles. Jpn. J. Physiol. 38, 819–838.
Nishimura, S., Kawai, Y., Nakajima, T., Hosoya, Y., Fujita, H., Katoh, M., Yamashita, H., Nagai, R., Sugiura, S., 2006. Membrane potential of rat ventricular myocytes responds to axial stretch in phase, amplitude and speed-dependent manners. Cardiovasc Res. 72, 403–411.
Pathak, C.L., 1957. The influence of stretch stimuli on the chronotropic response of the frog's isolated whole heart and its individual chambers. Indian J. Med. Sci. 11, 808–812.
Pellis, T., Kette, F., Lovisa, D., Franceschino, E., Magagnin, L., Mercante, W.P., Kohl, P., 2009. Utility of pre-cordial thump for treatment of out of hospital cardiac arrest: a prospective study. Resuscitation 80, 17–23.
Plank, G., Burton, R.A., Hales, P., Bishop, M., Mansoori, T., Bernabeu, M.O., Garny, A., Prassl, A.J., Bollensdorff, C., Mason, F., Mahmood, F., Rodriguez, B., Grau, V., Schneider, J.E., Gavaghan, D., Kohl, P., 2009. Generation of histo-anatomically representative models of the individual heart: tools and application. Philos. Trans. a Math. Phys. Eng. Sci. 367, 2257–2292.
Prosser, B.L., Ward, C.W., Lederer, W.J., 2011. X-ROS signaling: rapid mechano-chemo transduction in heart. Science 333, 1440–1445.
Quinn, T.A., 2014. The importance of non-uniformities in mechano-electric coupling for ventricular arrhythmias. J. Interv. Card. Electrophysiol. 39, 25–35.
Reed, A., Kohl, P., Peyronnet, R., 2014. Molecular candidates for cardiac stretch-activated ion channels. Global Cardiol. Sci. Practice 2, 19. http://dx.doi.org/10.5339/gcsp.2014.19.
Riemer, T.L., Tung, L., 2003. Stretch-induced excitation and action potential changes of single cardiac cells. Prog. Biophys. Mol. Biol. 82, 97–110.
Sachs, F., 2011. Cardiac Mechano-electric Coupling and Arrhythmias, second ed. Oxford University Press.
Sasaki, N., Mitsuiye, T., Noma, A., 1992. Effects of mechanical stretch on membrane currents of single ventricular myocytes of guinea-pig heart. Jpn. J. Physiol. 42, 957–970.
Seo, K., Inagaki, M., Nishimura, S., Hidaka, I., Sugimachi, M., Hisada, T., Sugiura, S., 2010. Structural heterogeneity in the ventricular wall plays a significant role in the initiation of stretch-induced arrhythmias in perfused rabbit right ventricular tissues and whole heart preparations. Circ. Res. 106, 176–184.
Shiels, H.A., White, E., 2008. The Frank-Starling mechanism in vertebrate cardiac myocytes. J. Exp. Biol. 211, 2005–2013.
Solovyova, O., Katsnelson, L.B., Konovalov, P.V., Kursanov, A.G., Vikulova, N.A., Kohl, P., Markhasin, V.S., 2014. The cardiac muscle duplex as a method to study myocardial heterogeneity. Prog. Bio. Mol. Biol. 115 (2-3), 115–128. http://dx.doi.org/10.1016/j.pbiomolbio.2014.07.010.
Suchyna, T.M., Johnson, J.H., Hamer, K., Leykam, J.F., Gage, D.A., Clemo, H.F., Baumgarten, C.M., Sachs, F., 2000. Identification of a peptide toxin from Grammostola spatulata spider venom that blocks cation-selective stretch-activated channels. J. Gen. Physiol. 115, 583–598.
Sung, D., Mills, R.W., Schettler, J., Narayan, S.M., Omens, J.H., McCulloch, A.D., 2003. Ventricular filling slows epicardial conduction and increases action potential duration in an optical mapping study of the isolated rabbit heart. J. Cardiovasc. Electrophysiol. 14, 739–749.
Tavi, P., Han, C., Weckstrom, M., 1998. Mechanisms of stretch-induced changes in $[Ca^{2+}]_i$ in rat atrial myocytes: role of increased troponin C affinity and stretch-activated ion channels. Circ. Res. 83, 1165–1177.
ter Keurs, H.E., Shinozaki, T., Zhang, Y.M., Zhang, M.L., Wakayama, Y., Sugai, Y., Kagaya, Y., Miura, M., Boyden, P.A., Stuyvers, B.D., Landesberg, A., 2008. Sarcomere mechanics in uniform and non-uniform cardiac muscle: a link between pump function and arrhythmias. Prog. Biophys. Mol. Biol. 97, 312–331.
Thompson, S.A., Copeland, C.R., Reich, D.H., Tung, L., 2011. Mechanical coupling between myofibroblasts and cardiomyocytes slows electric conduction in fibrotic cell monolayers. Circulation 123, 2083–2093.
Tohse, N., 1990. Calcium-sensitive delayed rectifier potassium current in guinea pig ventricular cells. Am. J. Physiol. 258, H1200–H1207.
Trayanova, N., Li, W., Eason, J., Kohl, P., 2004. Effect of stretch-activated channels on defibrillation efficacy. Heart Rhythm 1, 67–77.
Tsai, C.T., Chiang, F.T., Tseng, C.D., Yu, C.C., Wang, Y.C., Lai, L.P., Hwang, J.J., Lin, J.L., 2011. Mechanical stretch of atrial myocyte monolayer decreases sarcoplasmic reticulum calcium adenosine triphosphatase expression and increases susceptibility to repolarization alternans. J. Am. Coll. Cardiol. 58, 2106–2115.
Tung, L., Zou, S., 1995. Influence of stretch on excitation threshold of single frog ventricular cells. Exp. Physiol. 80, 221–235.
Van Wagoner, D.R., Lamorgese, M., 1994. Ischemia potentiates the mechanosensitive modulation of atrial ATP-sensitive potassium channels. Ann. N. Y. Acad. Sci. 723, 392–395.
von Lewinski, D., Kockskamper, J., Pieske, B., 2005. Stretch-induced slow force response in mammalian ventricular myocardium. In: Kamkin, A., Kiseleva, I. (Eds.), Mechanosensitivity in Cells and Tissues. Moscow.
Wang, K., Lee, P., Mirams, G., Gavaghan, D.J., Kohl, P., Bollensdorff, C., 2014. Reliable extraction of action potential and calcium transient data from guinea pig and rabbit ventricular tissue slices. Am. J. Physiol. (in review).
Ward, M.L., Williams, I.A., Chu, Y., Cooper, P.J., Ju, Y.K., Allen, D.G., 2008. Stretch-activated channels in the heart: contributions to length-dependence and to cardiomyopathy. Prog. Biophys. Mol. Biol. 97, 232–249.
Waxman, M.B., Wald, R.W., Finley, J.P., Bonet, J.F., Downar, E., Sharma, A.D., 1980. Valsalva termination of ventricular tachycardia. Circulation 62, 843–851.
Werdich, A.A., Brzezinski, A., Jeyaraj, D., Khaled Sabeh, M., Ficker, E., Wan, X., McDermott Jr., B.M., Macrae, C.A., Rosenbaum, D.S., 2012. The zebrafish as a novel animal model to study the molecular mechanisms of mechano-electrical feedback in the heart. Prog. Biophys. Mol. Biol. 110, 154–165.
White, E., Le Guennec, J.Y., Nigretto, J.M., Gannier, F., Argibay, J.A., Garnier, D., 1993. The effects of increasing cell length on auxotonic contractions; membrane potential and intracellular calcium transients in single guinea-pig ventricular myocytes. Exp. Physiol. 78, 65–78.
Woods, C.E., Novo, D., DiFranco, M., Vergara, J.L., 2004. The action potential-evoked sarcoplasmic reticulum calcium release is impaired in mdx mouse muscle fibres. J. Physiol. 557, 59–75.
Xie, Y., Garfinkel, A., Camelliti, P., Kohl, P., Weiss, J.N., Qu, Z., 2009. Effects of fibroblast-myocyte coupling on cardiac conduction and vulnerability to reentry: a computational study. Heart Rhythm 6, 1641–1649.
Yang, X.C., Sachs, F., 1989. Block of stretch-activated ion channels in *Xenopus oocytes* by gadolinium and calcium ions. Science 243, 1068–1071.
Yasuhara, S., Takaki, M., Kikuta, A., Ito, H., Suga, H., 1996. Myocardial VO_2 of mechanically unloaded contraction of rat ventricular slices measured by a new approach. Am. J. Physiol. 270, H1063–H1070.
Youm, J.B., Han, J., Kim, N., Zhang, Y.H., Kim, E., Leem, C.H., Kim, S.J., Earm, Y.E., 2005. Role of stretch-activated channels in the heart: action potential and Ca^{2+} transients. In: Kamkin, A., Kiseleva, I. (Eds.), Mechanosensitivity in Cells and Tissues. Moscow.
Zabel, M., Koller, B.S., Sachs, F., Franz, M.R., 1996. Stretch-induced voltage changes in the isolated beating heart: importance of the timing of stretch and implications for stretch-activated ion channels. Cardiovasc Res. 32, 120–130.
Zeng, T., Bett, G.C., Sachs, F., 2000. Stretch-activated whole cell currents in adult rat cardiac myocytes. Am. J. Physiol. Heart Circ. Physiol. 278, H548–H557.
Zhan, H., Xia, L., 2013. Excitation-contraction coupling between human atrial myocytes with fibroblasts and stretch activated channel current: a simulation study. Comput Math. Methods Med. 2013, 238676.
Zhang, Y., Sekar, R.B., McCulloch, A.D., Tung, L., 2008. Cell cultures as models of cardiac mechanoelectric feedback. Prog. Biophys. Mol. Biol. 97, 367–382.
Zhang, Y.H., Youm, J.B., Sung, H.K., Lee, S.H., Ryu, S.Y., Ho, W.K., Earm, Y.E., 2000. Stretch-activated and background non-selective cation channels in rat atrial myocytes. J. Physiol. 523 (Pt 3), 607–619.